Short Communication

Enhanced Performance of TiO$_2$/α-Fe$_2$O$_3$ Nanostructure as Anode Material for Lithium-ion Batteries

Qi Cheng[1], Cheng Liu[1], Kun Meng[1], Xiaohua Yu[1*], Yannan Zhang[1], Jianxiong Liu[1], Xin Jin[2], Liying Jin[3]*

[1] National Engineering Research Center for solid waste, Kunming University of Science and Technology, Kunming 650093;
[2] Shanxi Enginerring Vocational College, Taiyuan 030009;
[3] Shandong Institute of Physical Education and Sports, Jinan 250102
[*]E-mail: mengkun010@163.com; xiaohua_y@163.com；

A novel lithium-ion anode material α-Fe$_2$O$_3$/TiO$_2$ is prepared by two-step hydrothermal method with pure titanium sheet, NaOH, and FeCl$_3$ solution. The nanocomposite material has been fully characterized by SEM, TEM EDX and XRD. The electrochemical performance of α-Fe$_2$O$_3$/TiO$_2$ nanocomposite as anode material in lithium ion batteries (LIB) are measured by battery test system and electrochemical workstation. The results demonstrate that the α-Fe$_2$O$_3$/TiO$_2$ nanocomposite is consisted of TiO$_2$ sheets and Fe$_2$O$_3$ particles on the surface. The electrode exhibits excellent electrochemical performance with capacity retention of 638 mAh/g after 30 cycles at 33.5 mA/g.

1. INTRODUCTION

Due to its high energy density and long cycle life, rechargeable lithium-ion batteries (LIBs) have attracted more attention in the past few decades and widely used in automobiles, electric vehicles and energy storage [1,2]. However, with the rapid development of other emerging industries, the capacity and cycle performance of lithium-ion batteries can not meet the actual needs [3,4]. The research shows that the lithium-ion anode material restricts the specific capacity and cycle performance. It is one of the hottest topics in lithium-batteries research [5,6].

Metal oxide has many virtues such as high specific capacity, non-toxic, easy to synthesis and low processing cost. It is considered as an ideal anode material for new generation lithium ion batteries[7,8]. On the one hand, it is generally accepted that TiO$_2$ based anode materials have low price, safe working potential and small volume change during charging and discharging, so the

foreground is attractive [9]. On the other hand, the theoretical capacity of transition metal oxide Fe_2O_3 as high as 1005 mAh/g. Gao et al [10] conducted the research on α-Fe_2O_3 anode material and found that the specific capacity remained at about 710 mAh/g. However, with cycle number increase, micro structure is prone to damage during working process, which lead to sharp capacity degradation [11,12].

Hence, we put forward a strategy of novel lithium-ion batteries anode materials with high specific capacity and good cycle stability. In this work, surface modification of TiO_2 materials with α-Fe_2O_3 was proposed. Because the surface area of TiO_2 material has a significant influence on the intercalation and removal of lithium ion, hydrothermal method was used to prepare TiO_2 nano precursor with high surface area. The surface morphology and composition of the sample were analyzed by scanning electron microscopy (SEM), energy dispersive spectroscopy (EDS) and transmission electron microscopy (TEM). The phase composition of the sample was studied by X ray diffraction (XRD). The electrochemical impedance performance and electrode performance of lithium batteries of the sample were investigated using a battery test system and an electrochemical workstation.

2. MATERIALS AND METHODS

2.1 Material preparations

The pure titanium sheet (Sumitomo Group, Japan, chemical composition shown in Table 1) was cut into size 30 mm × 80 mm×1 mm and then placed in acetone, absolute ethanol and distilled water for 15 min each with ultrasonic vibration. The titanium sheet was chemically polished to remove the oxide film in the mixed solution of HF, HNO_3 and H_2O (volume ratio 1:1:8), then washed by distilled water and put in a dry oven.

Table 1. The chemical composition of pure titanium (mass percent %)

O	N	C	H	Fe	Si	Ti
0.15	0.05	0.05	<0.015	<0.30	<0.15	other

The titanium sheet and NaOH solutions (1 mol/L, 80 ml) were placed in a teflon-lined autoclave (100 ml) and treated at 180°C for 12 h to obtain a TiO_2 nanostructure. That is the first hydrothermal reaction. The resultant precipitation at the bottom was added to a mixture of $FeCl_3$ (0.15 mol/L, 20 ml) and $NaNO_3$ (1 mol/L, 20 ml). Then the mixture was carried on the second hydrothermal reaction in teflon-lined autoclave at 100°C for 2.5 h. The products were collected by centrifugation, washed with deionized water for 3 times and then dried in vacuum oven at 80°C for 24 h. Finally, the as-collected products were annealed in a tube furnace at 400°C at a rate of 3°C/ min.

2.2 Material characterizations

The surface morphology was characterized by scanning electron microscopy (SEM, LEO 1530Vp) with acceleration potential of 5 kV and transmission electron microscopy (TEM, Tecnai G2

20 S-TWIN). The phase composition of the sample was analyzed by X ray diffraction (XRD, D8 ADVANCE) with Cu Kα 1486.6 eV, λ = 0.15406 nm, operating voltage was 30 kV and the current is 30 mA. XRD peaks were collected from 20° to 80° with a step size of 0.5^o.

2.3 Electrochemical characterization

CR2025 coin-type cells were assembled in an argon-filled glove box (America, Innovative Technology, O_2 <1 ppm, H_2O<1 ppm). The anode electrode was prepared by mixing the Li4Ti5O12 powder, carbon black and polyvinylidenefluoride with a weight ratio of 8:1:1 in N-methyl pyrrolidinone. The mixture was pasted on pure Cu foil and dried under vacuum at 60^oC for 12 h. A piece offlesh lithium metal was used as the counter electrode. Celgard 2400 membrane was used as the separator and 1 M LiPF6 solution in DMC/EC/DEC (1:1:1 in volume) was used as the electrolyte. The electrochemical characterization was carried out by galvanostatic cycling under 33.5 mA/g current densities between 0 and 3 V using a battery testing system (CT-3008 5V 10 mA, Neware). The cyclic voltammetry and electrochemical impedance spectrum (EIS) was conducted using a CHI 760E(China, Shanghai Chenhua ltd.) electrochemical workstation at room temperature.

3. RESULTS AND DISCUSSION

3.1 Morphology analysis

The microstructure of anode materials is directly related to the intercalation and deintercalation of lithium ions, which has a great influence on the electrical properties of lithium-ion batteries. Many scholars believe that with the increase of the anode materials surface area, the electrode performance in lithium batteries becomes better [13-16]. Fig. 1a presents the image of SEM and TEM of sample after one step hydrothermal reaction. Fig.1b shows SEM of sample after two-step hydrothermal reaction. As can be seen from these figures, the micromorphology of anode materials has also changed greatly with different hydrothermal times.

In Fig.1a, The product is in layered shape. Each layer is about 5 μm in size and about 20 nm in thickness. As can be seen from the local magnification, there are nanowires near the layer. Further amplification observation shows that nanowire (possibly TiO_2 nanotube) has a width of 2-3 nm and a length of 150 nm. To summarize, the layer is formed by interweaving of substantial nanowires in three-dimensional space. It can also induce a bird's nest shape nanostructure with the aid of mechanical external force [17-20]. The nanostructured material has a large specific surface area, because each nanotube is exposed [21-24].

In Fig. 1b, there are small particles with large fluctuations, and the particles are spherical, uniform in size and well distributed. The pores in the product are still a lot. As measured by a ruler, the size of each spherical particle is within the range of 30-130 nm. The specific surface area of nanosheet was increased by surface modification of α-Fe_2O_3. Similar morphology was also noted in Wang's research, but differ from nanotube structure reported, diameter of particles here are bigger. That means particles may accumulate on the surface of nanosheets[25].
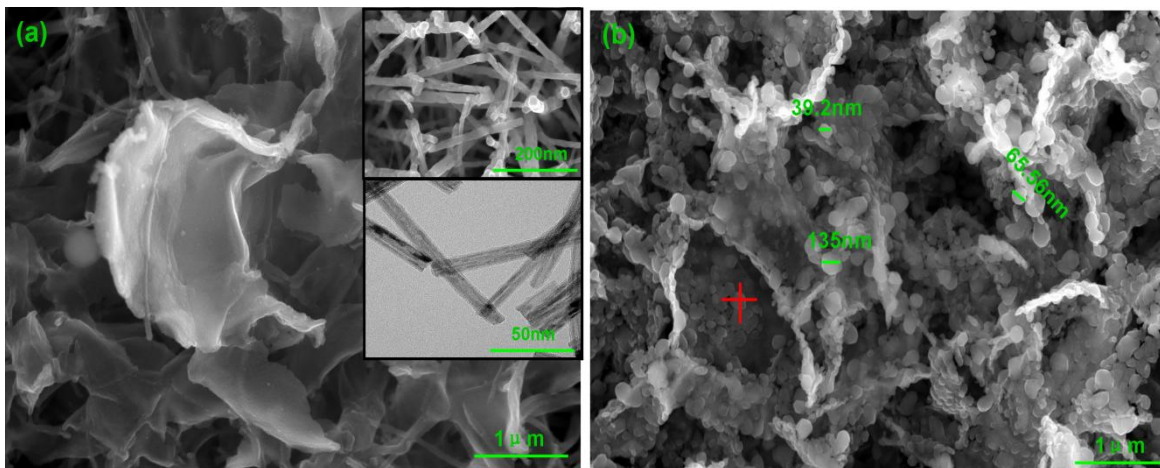
Figure 1. The image of SEM and TEM (a) one step hydrothermal reaction, (b) two-step hydrothermal reaction

Fig. 2 is the EDS micro elemental analysis diagram at the marked points in Fig. 1b. The main elements in the diagram are Fe, Ti, and O elements. Therefore, it can be preliminarily concluded that the α-Fe$_2$O$_3$ nanocomposite with TiO$_2$ matrix is formed.

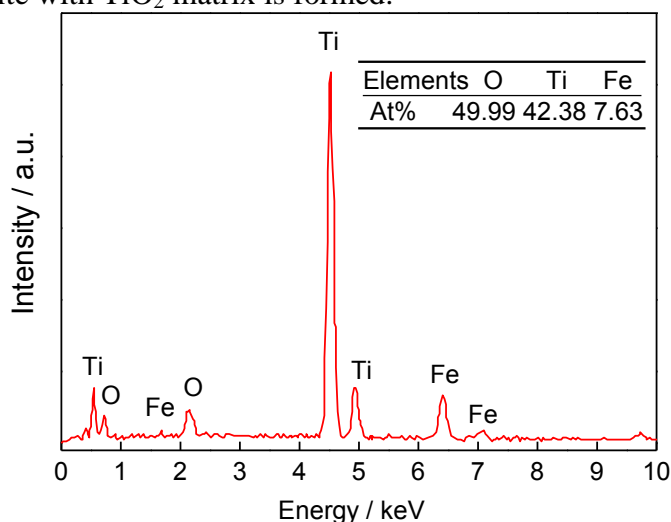| Elements	O	Ti	Fe
At%	49.99	42.38	7.63

Figure 2. Micro component of sample after two-step hydrothermal reaction

3.2 phase composition analysis

X-ray diffraction (XRD) measurements were conducted to determine the crystal structures of the nanostructures, which had been synthesized. The XRD spectra of supernatant (a) and precipitate (b) of the two-step hydrothermal products after annealing are given in Fig. 3. The XRD pattern of the pristine Fe$_2$O$_3$ nanorods exhibited four peaks at 2θ=36°, 43.5°, 62.4°and 63.9° assigned to the (110), (202), (214), and (300) reflections, respectively, of α-Fe$_2$O$_3$ with lattice constants: a=0.504 nm and c=1.375 nm (JCPDS no.89-2810). The XRD pattern of the α-Fe$_2$O$_3$/TiO$_2$ showed two small broad extra

reflection peaks at $2\theta=48.1°$ and $75.2°$ assigned to (200) and (215) reflections, respectively, of body-centered tetragonal-structured anatase TiO_2 with lattice constants: $a=0.3777$ nm and $c=0.9501$ nm (JCPDS no.89-4921). All of the reflection peaks were indexed to the planes of α-Fe_2O_3 and TiO2, suggesting that the synthesized nanoparticles are highly pure nanocomposite of them.
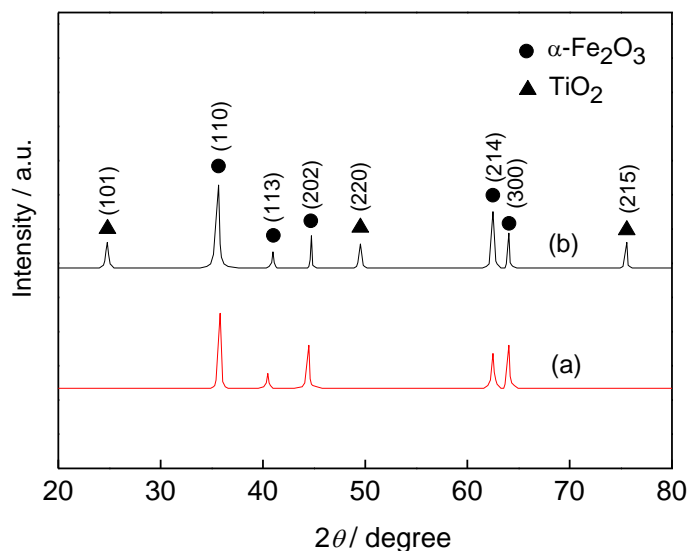

Figure 3. XRD patterns of samples after two-step hydrothermal reaction
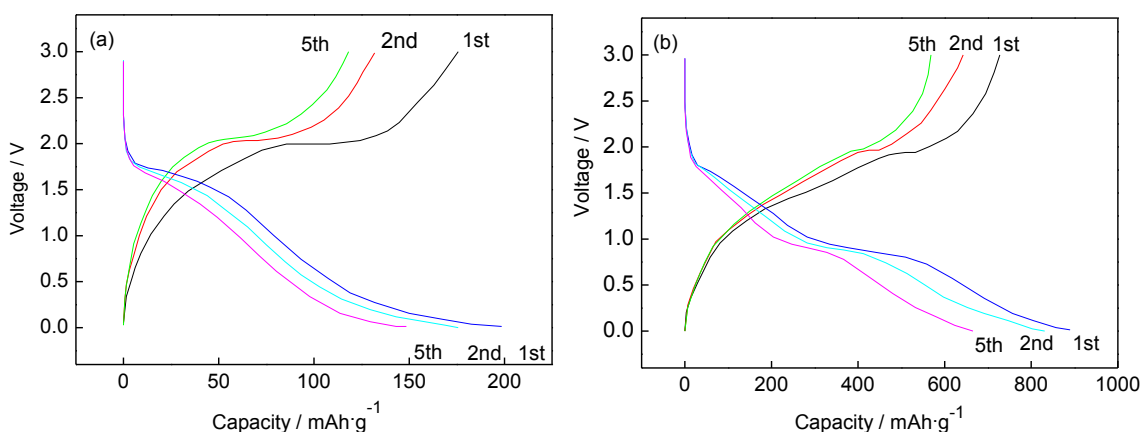
3.3 Electrochemical performance

Figure 4. The discharge-charge curves at 0.1 C current density (a) TiO_2 (b) α-Fe_2O_3/TiO_2

Fig. 4 shows the charge and discharge curves for the first five times of the TiO_2 nanostructure and the α-Fe_2O_3/TiO_2 nanocomposite with a voltage range of 0~3 V. Due to the presence of iron oxides, the α-Fe_2O_3/TiO_2 sample exhibits high initial discharge and charge capacities of 881 mAh/g; whereas the bare TiO_2 nanostructure can only deliver nearly one-third of the values (Fig. 4a). The irreversible capacity loss of 27% may be mainly attributed to irreversible processes such as the inevitable formation of inorganic solid electrolyte interface (SEI) film and electrolyte decomposition, which are common to most anode materials[26]. Compared with pure TiO_2 nanostructure, the capacity

of α-Fe_2O_3/TiO_2 nanocomposite has been greatly improved. In addition, the discharge process of α-Fe_2O_3/TiO_2 nanocomposite is gentler than that of TiO_2 nanostructure. There are two discharge platforms in the discharge curve, which means that the surface modification of TiO_2 nanostructure can effectively improve the electrical properties.

Fig. 5 shows the 30 times discharge cycling performance test curves of the pure TiO_2 nanostructure and the α-Fe_2O_3/TiO_2 nanocomposite at 0.1C. The residual capacity of the pure TiO_2 nanostructure is 136 mAh/g, and irreversible capacity loss is 31%. While the residual capacity of the α-Fe_2O_3/TiO_2 nanocomposite is 638 mAh/g, and the irreversible capacity loss is 27%. That is, the cyclic stability of the α-Fe_2O_3/TiO_2 nanocomposite is higher than the cyclic stability of the pure TiO_2 nanostructure. In consideration of large volume change of metallic oxide during charge and discharge, this result is superior to most reported TiO_2-based 3D electrodes[27,28].
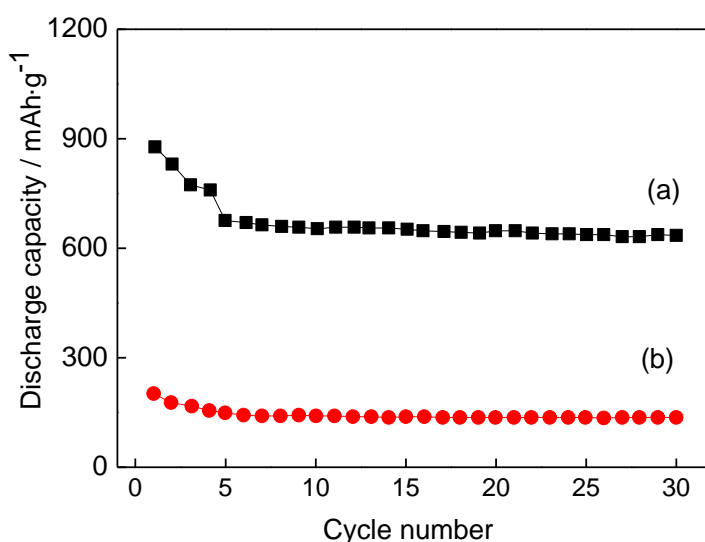

Figure 5. The cycle performance test curve (a) TiO_2, (b) α-Fe_2O_3/TiO_2

Generally , excellent electrode materials has a reversible oxidation reduction reaction in lithium batteries [29,30]. In our present work, the degree and reversibility of redox reaction on the electrode surface were measured by cyclic voltammetry, and the electrochemical performance of the electrode was characterized. Fig. 6 shows the cyclic voltammetry curves for TiO_2 nanostructure and α-Fe_2O_3/TiO_2 nanocomposite. The two samples have similar redox peaks, and this process also corresponds to the intercalation and deintercalation process of lithium ions.

Table 2 summarizes some recent studies of TiO_2/metal oxide hybrids as anodes for lithium-ion batteries. The specific capacity of our α-Fe_2O_3/TiO_2 is higher than those reported values for TiO_2@metal oxide hybrids at similar current densities. Besides, our TiO_2/Fe_2O_3 hybrid also exhibit small particle size and good cycling stability. The α-Fe_2O_3/TiO_2 electrode exhibits large reversible capacity as well as good cycling stability and rate performance, which can be attributed to its unique hierarchical architecture and synergistic effects between the constituents of the composite. First, TiO_2 nanosheet can build up a stable 3D scaffold for the growth of Fe_2O_3 which can deliver large capacity for energy storage. Our α-Fe_2O_3/TiO_2 contribute a larger capacity to the hybrid electrode compared to

most previous studies of anatase TiO_2, second only to TiO_2-B nanowire@α-Fe_2O_3. As TiO_2-B has a more open structure than anatase TiO_2, TiO_2-B nanowire@α-Fe_2O_3 shown in ref [1] delivers large capacity up to 709 mAh/g. Second, the smallest particle in our design could facilitate the electrolyte penetration by providing a large reaction surface area and more active sites for electrochemical reactions, which facilitates fast charge transport at high current densities. Last, the small dimensions and the hollow interiors of the Fe_2O_3 not only provide short Li^+ ion diffusion paths, but also improve sufficient structural stability to withstand the large volume change associated with Li insertion/extraction.

Table 2. List of recent studies of TiO_2/metal oxides as anodes for lithium ion batteries

morphology	crystallite size	current rate (mA g^{-1})	cycles number	reversible capacity (mA·hg^{-1})	ref
TiO_2-B nanowire @α-Fe_2O_3	100 -200 nm	100	50	709	[15]
sandwich-like Co_3O_4/TiO_2	20-40 μm	100	120	660	[31]
TiO_2@Fe_2O_3 Core-Shell	around 100 nm	100	100	520	[32]
TiO_2@MnO_2	around 81 nm	335	100	350	[33]
TiO_2@Fe_2O_3 nanotube	about 100 nm	100	100	617	[34]
TiO_2/α-Fe_2O_3	30-130 nm	33.5	30	638	This work

In Fig. 6a, the highest point is about 2.27 V, and the peak value generated by oxidation is corresponding to the prolapse process of lithium ions (the charging process), while the lowest point is about 1.57 V, which corresponds to the intercalation process of lithium ions (the discharge process). The peak value of the oxidation peak is basically symmetrical with the peak value of the reduction peak, and the integral area is approximately equal, indicating that the oxidation and reduction are basically consistent during charging and discharging. In Fig. 6b, the highest point is about 2.25 V, the lowest point is about 1.61 V, and the peak values of both are essentially symmetrical.

In addition, the oxidation peak current value (I_{pa}) and the reduction peak current value (I_{pc}) are often compared to reflect the reversibility of lithium-ion batteries. If the ratio of them is more closer to one, the reversibility of the material in charging and discharging is better[35]. According to the curve, the I_{pa}/I_{pc}=0.68 of pure TiO_2 nanostructure and the I_{pa}/I_{pc} =0.98 of α-Fe_2O_3/TiO_2 nanocomposite are calculated, which shows that the coating modification is helpful to the improvement of the cycle performance. Moreover, the difference between the oxidation peak and the reduction peak of pure TiO_2 nanostructure is 0.705 V, which is slightly higher than that of α-Fe_2O_3/TiO_2 nanocomposite. This also shows that the α-Fe_2O_3/TiO_2 nanocomposite has less polarization effect on the electrolyte, and the performance is more stable.
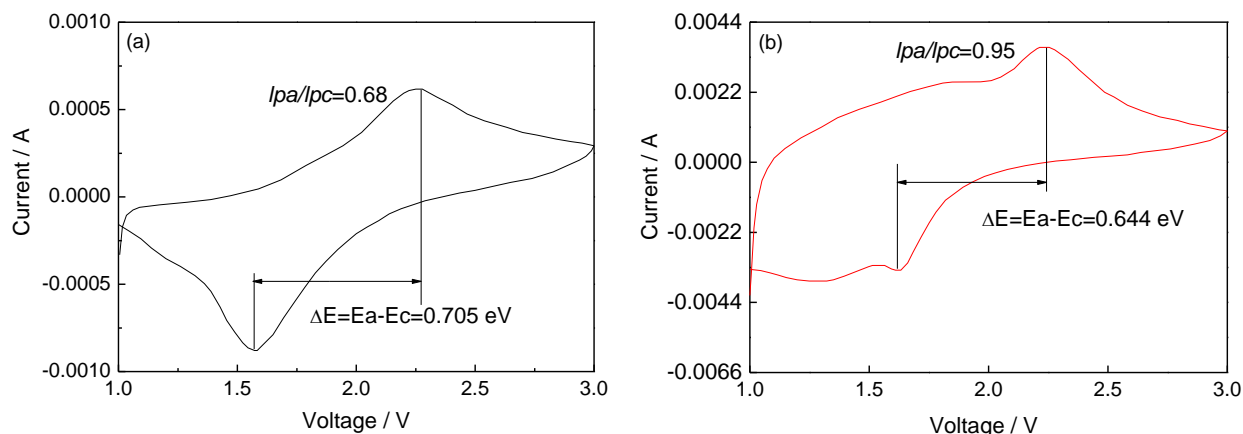
Figure 6. Cyclic voltammetry curves of samples after two-step hydrothermal reaction. (a) pure TiO_2 (b) α-Fe_2O_3/TiO_2

Electrochemical impedance measurement (EIS) is one of the important methods to characterize the charge diffusion and propagation resistance of a battery. It can effectively reflect the magnitude of the resistance of the battery. Electrochemical impedance diagram can be divided into two parts. The first part is the high frequency region, the shape of which is basically semicircle. The second part is low frequency area, and its shape is basically a diagonal shape[36]. The high frequency region mainly represents the resistance of the electrode surface charge transfer, and the low frequency region mainly represents the Warburg resistance of lithium ions in the electrode. The smaller the radius of the high frequency zone, the smaller the resistance, and the smaller the slope of the low frequency region is, the smaller the resistance[37].
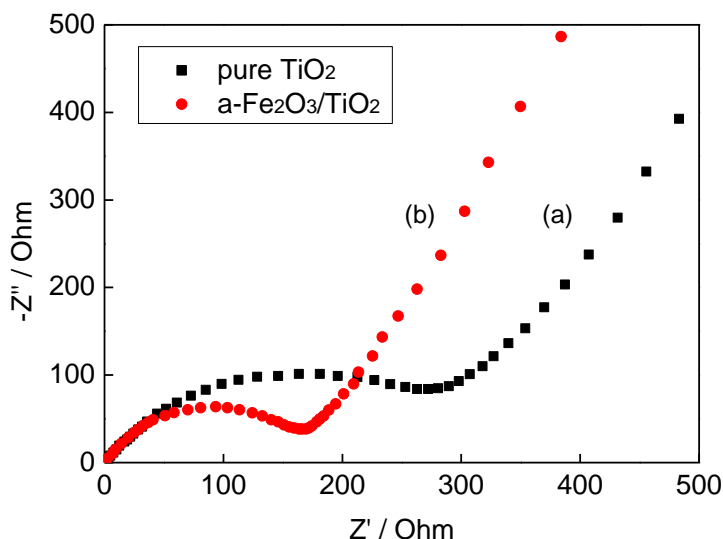

Figure 7. Electrochemical impedance curves of samples after two step hydrothermal reaction (a) pure TiO_2 (b) α-Fe_2O_3/TiO_2

Fig. 7 shows the electrochemical impedance curves of pure TiO_2 nanostructure and α-Fe_2O_3/TiO_2 nanocomposite. Comparing the trends in the graph, we can find that: 1) the radius of pure

TiO$_2$ nanostructure in the high frequency region is less than the radius of α-Fe$_2$O$_3$/TiO$_2$ nanocomposite; 2) the slope of line in low-frequency region of pure TiO$_2$ nanostructure is also smaller than that of α-Fe$_2$O$_3$/TiO$_2$ nanocomposite in the low frequency region. That means α-Fe$_2$O$_3$/TiO$_2$ nanocomposite exhibits larger Li-ion diffusion rate than pure TiO$_2$ nanostructure[38-39].

4. CONCLUSIONS

1) TiO$_2$ nanostructure and α-Fe$_2$O$_3$/TiO$_2$ nanocomposite were successfully prepared by the two-step hydrothermal reaction. TiO$_2$ nanostructure is formed by interweaving a large number of nanowires in three-dimensional space, and there are a lot of small particles on α-Fe$_2$O$_3$/TiO$_2$ nanocomposite. The specific surface area increased.

2) the α-Fe$_2$O$_3$/TiO$_2$ sample exhibits favarable initial discharge and charge capacities of 881 mAh/g; whereas the bare TiO$_2$ nanostructure can only deliver nearly one-third of the values.

3) In comparison with the TiO$_2$ nanostructure sample, The difference between the oxidation peak and the reduction peak of theα-Fe$_2$O$_3$/TiO$_2$ nanocomposite is smaller, and the impedance of the modified material in the high frequency region and the low frequency region are both decreased.

References

1. J.M. Liu, Y.J. Zhang, P. Dong, X. Li and S.B. Xia, *J. Chin. Ceram. Soc.,* 7 (2016) 4.
2. G.F. Ortiz, I. Hanzu, P. Lavela, P. Knauth, J.L. Tirado and T. Djenizian, *Chem. Mater.,* 22 (2010) 1926.
3. J. Chen, L. Xu, W. Li and X. Gou, *Adv. Mater.,* 17 (2005) 582.
4. M. D. Ye, X.K. Xin, C.J. Lin and Z.Q. Lin, *Nano Lett.,* 11 (2011) 3214.
5. I.A.J. Gordon, S. Grugeon, H. Takenouti, B.Tribollet, M. Armand, C. Davoisne, A. Débart and S. Laruelle, *Electrochim. Acta.,* 223 (2017) 63.
6. J.Y. Li, Q. Xu, G. Li, Y.X. Yin, L.J. Wan and Y.G. Guo, *Mater. Chem. Front.,* 1 (2017) 1691.
7. T.C. Jiang, F.X. Bu, X.X. Feng, I. Shakir, G.L Hao and Y.X. Xu, *Acs. Nano.,* 11 (2017) 5140.
8. A.A. Abdelhamid, Y. Yu, J. Yang and J.Y. Ying, *Adv. Mater.,* 29 (2017) 1701427.
9. M.X. Jing, J.Q. Li, C. Han, S.S. Yao, J. Zhang, H.A. Zhai, L.L. Chen, X.Q. Shen and K.S. Xiao, *Roy. Soc. Open. Sci.,* 4 (2017) 170323.
10. L. Zhang, G. Zhang, H.B. Wu, L. Yu and X.W. Lou, *Adv. Mater.,* 25 (2013) 2589.
11. J. Chen, L. Xu, W. Li and X. Gou, *Adv. Mater.,* 17 (2005) 582.
12. C.Z. Wu, P. Yin, X. Zhu, C.Z. Ouyang and Y. Xie, *J. Phys. Chem. B,* 110 (2006) 17806.
13. X.H. Yu and Z. L. Zhan, *Nanoscale Res. Lett.* 9 (2015) 516.
14. J. Wei, J.X. Liu, Z.Y. Wu, Z.L. Zhan, J. Shi and K. Xu, *J. Nanosci. Nanotechnol.,* 15 (2015) 5013.
15. X. Wang, J. Rong, Y. M. Song, X. H. Yu, Z. L. Zhan, J. S. Deng, *Physics Letters A,* 381 (2017) 2845.
16. X.H. Yu, J. Rong, Z.L. Zhan, Z. Liu, J.X. Liu, *Mater. Design.* 83 (2015) 159.
17. J. Jannik and J. Maier, *Cheminform,* 5 (2003) 5215.
18. H.L. Wang, Y. Yang, Y.Y. Liang, J.T. Robinson, Y.G. Li, A. Jackson,Y Cui and H.J. Dai, *Nano Lett.,* 11 (2011) 2644.

19. C. Liu, J. Rong, Y.N. Zhang, X.H. Yu, J.X. Liu and Z.L. Zhan, *Int. J. Electrochem. Sci.,* 12 (2017) 9914.
20. T. Song, J.L. Xia, J.H. Lee, D.H. Lee, M.S. Kwon, J.M. Choi, J. Wu, S.K. Doo, H. Chang, W.I. Park, D.S. Zang, H.S. Kim, Y.G. Huang, K.C. Hwang, J.A. Rogers and U. Paik, *Nano Lett.,* 10 (2010) 1710.
21. P. Poizot, S. Laruelle, S. Grugeon, L. Dupont and J.M. Tarascon, *Nature,* 407 (2000) 496.
22. T. Ohzuku, S. Takeda and M. Iwanaga, *J. Power Sources,* 81 (1999) 90.
23. S.Y. Huang, L. Kavan, I. Exnar and M. Grätzel, *J. Electrochem. Soc.,* 142 (1995) L142.
24. W.S. Zhi, W.Y. Li, J.J. Cha, G.Y. Zheng, Y. Yang, M.T. Mcdowell, P.C. Hsu and Y. Cui, *Nat Commun.,* 4 (2013) 1331.
25. H.G. Wang, D.L. Ma, X.L. Huang, Y. Huang and X.B. Zhang, *Sci Rep-Uk.,* 2 (2012) 701.
26. L. Yu, Z.Y. Wang, L. Zhang, H.B. Wu and X.W. Lou, J. *Mater. Chem. A,* 1 (2013) 122.
27. J.S. Luo, X.H. Xia, Y.S. Luo, C. Guan, J.L. Liu, X.Y. Qi, C.F. Ng, T. Yu, H. Zhang and H.J. Fan, *Adv. Energy Mater.,* 3 (2013) 737.
28. Y. Piao, J. Kim, H. Bin Na, D. Kim, J.S. Baek, M.K. Ko, J.H. Lee, M. Shokouhimehr and T. Hyeon, *Nat. Mater.,* 7 (2008) 242.
29. G.F. Ortiz, I. Hanzu, T. Djenizian, P. Lavela, J.L. Tirado and P. Knauth, *Chem. Mater.,* 21 (2009) 63.
30. L.G. Xue, Z. Wei, R.S. Li, J.L. Liu, T. Huang and A.S. Yu, *J. Mater. Chem.,* 21 (2011) 3216.
31. W.T. Li, K.N. Shang, Y.M. Liu, Y.F. Zhu, R.H. Zheng, L.Z. Zhao, Y.W. Wu, L. Li, Y.H. Chu, J.H. Liang and G. Liu, *Electrochim. Acta,* 174 (2015) 985.
32. Y. Zhong, Y.F. Ma, Q.B. Guo, J.Q. Liu, Y.D. Wang, M. Yang and H. Xia, *Sci Rep.*, 7 (2017) 40927.
33. J.Y. Liao, D. Higgins, G. Lui, V. Chabot, X. Xiao and Z. Chen, *Nano Lett.*, 13 (2013) 5467.
34. N. Liu, J. Shen and D. Liu, *Electrochim. Acta*, 97 (2013) 271.
35. Y.F. Shi, B.K. Guo, S.A. Corr, Q.H. Shi, Y.S. Hu, K.R. Heier, L.Q. Chen, R. Seshadri and G.D. Stucky, *Nano Lett.,* 9 (2009) 4215.
36. S. Laruelle, S. Grugeon, P. Poizot, M. Dolle, L. Dupont and J.M. Tarascon, *J. Electrochem. Soc.,* 149 (2002) A627.
37. K.Y. Xie, Z.G. Lu, H.T. Huang, W. Lu, Y.Q. Lai, J. Li, L.M. Zhou and Y.X. Liu, *J. Mater. Chem.,* 22 (2012) 5560.
38. H.B. Wu, J. S. Chen, X.W. Lou and H.H. Hng, *Nanoscale,* 2011, 3, 4082.
39. Z.Y. Wang and X.W. Lou, *Adv. Mater.,* 24 (2012) 4124.